

Thermal Analysis of Semiconducting Polymer Crystals Free of a Mobile Amorphous Fraction

Ngoc A. Nguyen,* Roddel A. Remy, and Michael E. Mackay*

Cite This: *Macromolecules* 2021, 54, 2155–2161

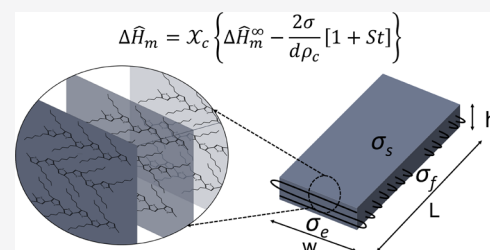
Read Online

ACCESS |

Metrics & More

Article Recommendations

ABSTRACT: Mobile-amorphous-free crystals of a semiconducting polymer, poly(3-hexyl thiophene) (P3HT), were made via a flow induced crystallization technique to yield crystals that were microns long while the other two dimensions were 6 and 21 nm in size. Thermal analysis revealed a melting point depression that is described by the Gibbs–Thomson (GT) equation resulting in an interpretation that is physically sound. On the contrary, contemporary analysis of the melting enthalpy, which also shows a depression below that for an infinitely sized crystal, yields results that are nonphysical and do not agree with the GT analysis. A simple argument is made to correct this discrepancy, using the first law of thermodynamics, to include the sensible heat of the molten crystal mass required for an extrapolation to the melting enthalpy of an infinitely sized crystal. A satisfactory comparison to the results from the GT equation is now found to reconcile older, literature data to good effect. However, the comparison is not as good for the P3HT crystals made here and believed to be because of the finite size of the crystals in two dimensions coupled with the rather large size of the polymer molecules prohibiting a continuum analysis.



INTRODUCTION

Single crystals have no amorphous content and do not exhibit glass transition, only a melting point. In addition to this unusual behavior, it is well known that the finite dimensions of single crystals, specifically the surface energies of the crystal faces, affect the melting temperature so it is below that for an infinitely sized crystal. Analysis of this effect is firmly embedded in the literature and understood through thermodynamics and a Gibbs free energy analysis to arrive at the Gibbs–Thomson (GT) equation. This analysis has been tested many times and the surface energies derived from it results in a good, physical interpretation.

The melting enthalpy shows similar behavior, however, interpretation is limited. Contemporary analysis of this effect is performed by imagining the infinitely sized crystal's melting enthalpy which is reduced by the surface energy of each crystal face appropriately scaled by its dimensions. This interpretation results in surface energies which are much higher than those derived from the melting point temperature depression and a nonphysical surface energy.

The challenge is an understanding of the melting enthalpy which has escaped quantitative discussion until now. An analysis of this effect is given here, utilizing the first law of thermodynamics, after a brief review of flow induced crystallization necessary to make the mobile-amorphous-free crystals for thermal analysis.

Shear or flow induced crystallization has been studied for many years with Pennings and coworkers^{1–4} being the first to crystallize polyethylene from dilute solution using flow.⁵ The key to crystal formation in this case was the lack of

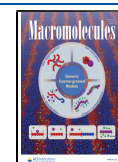
entanglements allowing extended chain crystals to be produced. Although the initial studies were performed in a shear apparatus, the concentric cylinder viscometer, crystallization did not occur until the critical Taylor number for secondary flow was reached at a certain apparent shear rate. The flow instability manifested as counter-rotating vortices to produce an elongation flow between them to stretch the macromolecules thereby producing stable, extended chain, crystals similar to the more straight-forward technique employed by McHugh and Schultz.⁶ It should be noted that the crystal structure observed by Pennings and co-workers was the shish-kebab where an oriented, extended chain, crystal (the shish) had nucleated lamellae (the kebab) along their length.

At the other end of the concentration scale is the polymer melt that is strongly entangled and the effect of orientation admitted during processing has also been found to strongly affect the crystallization kinetics and degree.^{7–11} In general, though, producing single crystals in the melt is not possible. Yet, unusual morphologies can be found since processing can introduce regions of high and low cooling rates together with regions of high and low deformation rates that both affect crystallization. For example, polymer melt injection molding

Received: November 9, 2020

Revised: February 3, 2021

Published: February 18, 2021



produces a region of high cooling rate coupled with a high deformation rate at the die surface to yield a skin region of highly oriented polymer.^{12–16} More recent studies^{17–19} found that the highly oriented skin layer can also contain shish-kebab structures that have kebabs nucleated from the oriented chains (shish) that incorporate all other chains as the extended chain crystals grow.

It is a challenge to produce single crystals in either concentration domain, especially at high concentration, or in the melt, homogeneously through a sample. Smith and Lemstra (and others)^{20–22} overcame this hurdle and reduced the entanglement effect by gel spinning the polymer. This was accomplished by dissolving the polymer in solvent then cooling it below the dissolution temperature. The result was a gel that had a reduced number of entanglements held together by small crystallites. The gel could be stretched to very high draw ratios yielding an incredibly strong fiber through molecular orientation.

In the present study, a combination of gel spinning and flow induced crystallization is used. Instead of forming a gel under quiescent conditions, the polymer is sheared while it crystallizes below the equilibrium dissolution temperature. The polymer used, poly(3-hexylthiophene) (P3HT), is known to crystallize as a long whisker,^{23–26} so, a resultant nano-fibrillar morphology is not unexpected. However, under the conditions of this study, we confirm the formation of mobile-amorphous-free crystal fibers through microscopy and thermal analysis. Further analysis is described elsewhere.²⁷ Herein, we also derive a more acceptable analysis of the crystal surface energy effect on the melting enthalpy of an infinitely sized crystal that produces a reliable interpretation of literature data. A first attempt at applying the new derivation to our mobile-amorphous-free P3HT crystals is also presented and discussed.

EXPERIMENTAL SECTION

P3HT (p100, M_w ~50 kDa, ~95% regioregularity) and 2-ethyl-naphthalene (2-EN with ca. 99% purity, 0.0229 mmHg vapor pressure at 25 °C) were purchased from BASF and Sigma-Aldrich, respectively. The chemicals were used without purification. P3HT was dissolved in 2-EN, 20 mg/mL, at 80 °C and 60 rpm on a hot plate for 3 h. After cooling to ambient temperature, the P3HT solution was sheared at a rate of 100 s⁻¹ under ambient temperature for 24 h using a strain-controlled rheometer (ARES-G2, TA instruments) with 25 mm parallel plates and 0.5 mm gap. The process is detailed in Ref 27. and 32. The sheared P3HT solution was spin coated on silicon wafers at 5000 rpm for 5 min for atomic force microscopy (AFM) characterization. Before spin coating, the silicon wafers were carefully cleaned with acetone and isopropyl alcohol for 15 min each by sonication (Cole- Palmer 8891). The cleaned silicon wafers were blown with air then placed in a vacuum oven at 40 °C. The AFM phase and height images were collected using a Veeco Dimension 3100 V in the tapping mode. Diluted sheared P3HT solutions were drop-cast onto ultrathin carbon support grids for transmission electron microscopy (TEM) and selected area electron diffraction analysis using a JEOL JEM-2010F High-Resolution TEM at 200 kV. The sheared solutions also were rapidly precipitated in methanol, then filtered and dried in a vacuum oven at room temperature for one week for complete drying. Temperature-modulated differential scanning calorimetry (TMDSC) was utilized to characterize the samples with a temperature ramp of 3 °C/min, oscillation frequency period of 30 s, and amplitude of 0.239 °C using a TA instruments Discovery Series DSC equipped with an RCS90 cooling accessory. For comparison of the melting endotherm, sheared and unsheared samples were also examined with standard DSC at 10 °C/min from -85 to 300 °C with a 50 mL/min nitrogen cell purge flow. In this study, the spin coated

samples were only used for AFM characterization. All DSC data were collected using the precipitated samples.

RESULTS AND DISCUSSION

The produced mobile-amorphous-free P3HT crystals are presented in Figure 1. Microns-long and ca. 21 nm wide

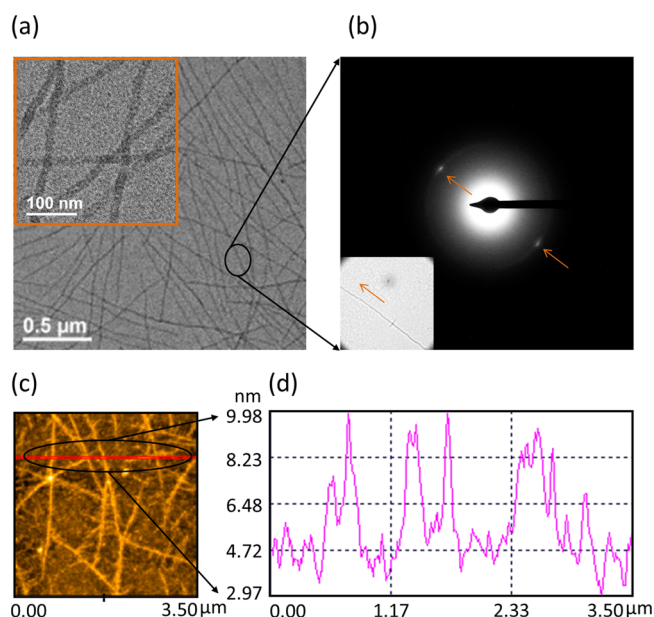


Figure 1. Mobile-amorphous-free P3HT crystals. (a) TEM image of P3HT crystals. (b) Selected area electron diffraction of a mobile-amorphous-free P3HT crystal indicating π - π stacking of thiophene rings along the fibril direction. (c) AFM height image of mobile-amorphous-free P3HT crystals. (d) P3HT fibril height that generated a large increase in viscosity. Similarly, Koppe et al.²⁹ sheared P3HT to produce what they called a gel, similar to our subsequent study. Here we consider the thermal properties of the crystals produced via shear.

crystal fibrils are observed clearly in the TEM images (Figure 1a). An example of selected area electron diffraction of an individual fibril (Figure 1b) demonstrates that the fibril has π - π stacking of thiophene rings aligned in only one direction, along the length of the fibril.²⁷ The AFM phase and height images of individual P3HT crystals are shown in Figure 1c. The small protrusions perpendicular to the main fibers in the AFM height image (Figure 1c) are likely residual polymer chains in the gel that crystallized during the spin coating process. These are clearly not observed in the TEM image (Figure 1a) of the fibers drop cast onto TEM grids. A line profile taken from Figure 1c shows a fibril thicknesses of ca. 6 nm (Figure 1d). In a previous publication²⁸ we sheared P3HT as it phase separated from the solution in 2-EN. The emphasis was to ascertain the effect of shear to produce a percolated network of crystal fibrils.

The results in Figure 2a show that the crystalline enthalpy of melting increases as the polymer is sheared while phase separating from 2-EN. The enthalpy is 13.7, 18.0, 19.3, and 25.3 J/g for the pristine (Pristine P3HT (as received)), dissolved then rapidly precipitated in methanol (Before shear), dissolved and aged for 24 h then rapidly precipitated (Storage), and after shearing at 100 s⁻¹ for 24 h (After shear), respectively. Even if a sample is not crystalline in solution one may expect that during precipitation it will achieve some crystallinity. Yet, it is expected that if a sample is fully

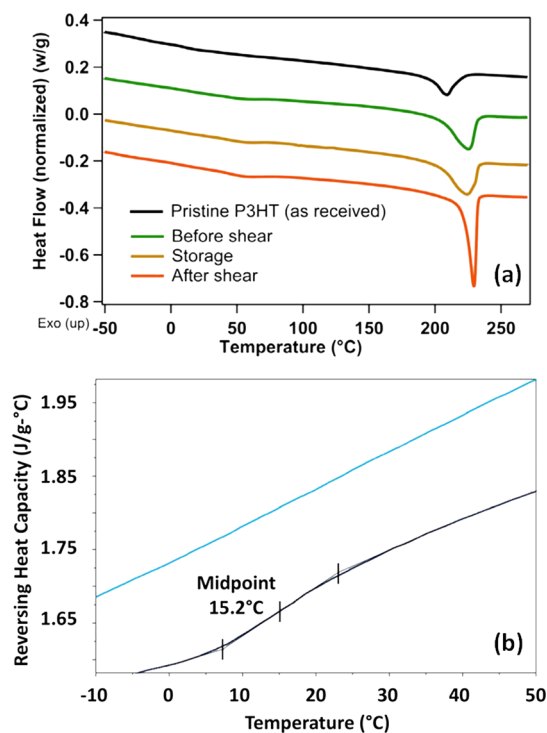


Figure 2. Differential scanning calorimetry results for P3HT prepared under different conditions. (a) Standard DSC for P3HT as received (Pristine P3HT (as received)) and dissolved in 2-EN then prepared to make a DSC sample immediately after preparation (Before Shear), stored for 24 h (Storage), and sheared for 24 h at 100 s^{-1} (After Shear). (b) Reversing heat capacity as a function of temperature for the After Shear sample (upper curve) and the Pristine sample (lower curve). A glass transition is not seen for the After Shear sample.

crystallized in solution it will not change after precipitation and it is impossible to manufacture a fully crystallized sample during precipitation. The glass transition of P3HT is very delicate and difficult to observe, but its absence would further confirm our claim of a mobile-amorphous-free, crystalline sample using shear. Therefore TMDSC was used to characterize it. The reversing heat capacity is shown in Figure 2b and for the pristine P3HT sample there is a clearly observable glass transition centered at $15.2\text{ }^{\circ}\text{C}$. Previous TMDSC analysis³⁰ showed that P3HT displays a two-step glass transition but this consideration is beyond the scope of this work. Conversely, the sheared sample does not exhibit a glass transition to the sensitivity of our instrument. This suggests there is no mobile amorphous content in the sample.

A very sharp melting transition is determined with DSC and there is no evidence of a glass transition even with the more sensitive TMDSC technique. Combined with the aforementioned TEM and AFM analysis we conclude that during shear crystallization, there is an Ostwald ripening process³¹ where continuous shear tears improperly incorporated chains from the growing large crystal until perfect crystals are formed throughout the solution.²⁷ Yet, the melting enthalpy is half the value determined through an employed extrapolation technique ($43 \pm 2\text{ J/g}$)³² in good agreement with a similar value found by others ($49 \pm 2\text{ J/g}$).³⁵ In this study, we use the term “mobile-amorphous-free crystals” to describe the P3HT crystals having no mobile amorphous fraction that was demonstrated through the unobserved glass transition temperature in the sheared sample. The polymer chains will adopt a

chain folded conformation during the crystallization process because of their high molecular weight.^{32,33} A representation of this chain folded crystal structure is shown for P3HT in Figure 3. The chain folds themselves represent a rigid amorphous

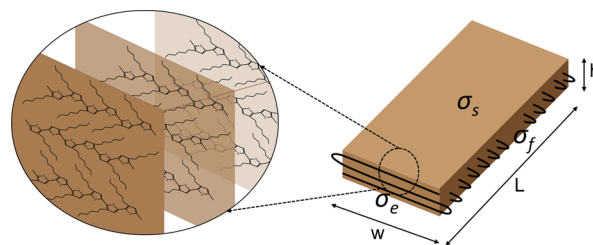


Figure 3. A crystal represented as a parallelepiped with length scales h , w , and L together with surface energies σ_f , σ_e , and σ_s . P3HT has the chain folds on the side surface as illustrated while polyethylene has folds on the surface characterized by σ_s . Zoomed-in section is the π - π stacking of the thiophene rings along the fibril axis.

phase and would contribute to the surface energy of the appropriate crystal faces from which they protrude. Thus, we were faced with the quandary of believing we have mobile-amorphous-free P3HT crystals, if not a single crystal, manufactured via an Ostwald ripening process, with an unexpectedly low melting enthalpy.

At the heart of Ostwald ripening is the GT equation^{34,35} that can be used to predict if smaller crystals are more soluble than larger ones. The equation relates the melting temperature of a finite size crystal, T_m , to that of an infinite size crystal, T_m^∞ , with the interfacial energy at the solid–liquid interface, $\sigma_{s,l}$

$$T_m = T_m^\infty - \frac{2\sigma_{s,l}V_s}{r\Delta S_m^\infty} \quad (1)$$

where V_s is the solid molar volume and ΔS_m^∞ is the molar entropy change of melting an infinite size crystal. This equation is strictly valid for a sphere of radius r and the difference of the two temperatures is related to the Laplace pressure which is appreciable for small crystals.³⁴

An infinitely sized crystal will have a change in molar enthalpy of melting, $\Delta H_m^\infty = T_m^\infty\Delta S_m^\infty$ at its melting temperature, since the Gibbs free energy of the solid and liquid will be the same at equilibrium. Applying this to eq 1 gives a more familiar form of the GT equation

$$T_m = T_m^\infty - \frac{2\sigma_{s,l}V_sT_m^\infty}{r\Delta H_m^\infty} \quad (2)$$

Since many crystals of macromolecules are rectangular parallelepipeds, produced by chain folding, this equation is frequently generalized to³⁴

$$T_m = T_m^\infty \left[1 - \frac{2\sigma_e}{L\rho_c\Delta\hat{H}_m^\infty} - \frac{2\sigma_s}{h\rho_c\Delta\hat{H}_m^\infty} - \frac{2\sigma_f}{w\rho_c\Delta\hat{H}_m^\infty} \right] \quad (3)$$

where crystal dimensions, h , w and L , shown in Figure 3, as are the energies associated with the fold (σ_f), end (σ_e), and lateral (σ_s) surfaces. The thiophene ring (π - π) stacking is parallel to the L -direction with a h and w of 6 and 21 nm, respectively. The crystal density ρ_c is used instead of the molar volume and the melting enthalpy is written on a per mass basis as $\Delta\hat{H}_m^\infty$ in the above equation.

Equation 3 has its roots in thermodynamics and has proven useful to determine the surface energy for polyethylene³⁶ as well as the distribution of lamellar thicknesses.³⁷ The polymers characterized in this way typically have large width (w) and length (L) compared to thickness (h) and the lamellar thickness is associated with this dimension. The simplest method to find the distribution is to use DSC and assume that the height of the melting endotherm at a given T_m is proportional to the fraction of lamellae of thickness h , see also Alberola et al.³⁸ One must know, or assume, T_m^∞ and σ_s to determine h (for polyethylene the folds are on the surface denoted by σ_s ; L and w are much larger than h).

As stated above, shearing produces long, thin, individual crystals for the system considered here. Other polymers have thin lamellae that are the building blocks of much larger spherulitic structures. Despite the lamellae forming large crystals, the energy required to melt the material is lower than expected. Thus, in addition to having a lower melting temperature, the melting enthalpy is also reduced from surface energetics and has been frequently written as³⁶

$$\Delta\hat{H}_m = \chi_c \left\{ \Delta\hat{H}_m^\infty - \frac{2\sigma_e}{L\rho_c} - \frac{2\sigma_s}{h\rho_c} - \frac{2\sigma_f}{w\rho_c} \right\} \quad (4)$$

where χ_c is the mass fraction of crystals and $\Delta\hat{H}_m$ is the melting enthalpy of a finite size crystal.

In this report, we suggest a different derivation using the first law of thermodynamics defining **state 1** as the crystals at the temperature (and pressure) just prior to the beginning of the melting endotherm and **state 2** at the extrapolated temperature T_m^∞ . Following the path from state 1 to 2, one arrives at

$$m\Delta\hat{H}_m + 2\sigma A_c + m_c C_{pl}[T_m^\infty - T_m] = m_c \Delta\hat{H}_m^\infty \quad (5)$$

with m_c representing the mass of crystals in the sample, m , the total sample mass, C_{pl} the liquid heat capacity on a mass basis, and σA_c is shorthand for summation of the surface energy for a given crystal face times its area. The term $m\Delta\hat{H}_m$ has m rather than m_c because of the definition of the melting enthalpy with units of Joules per total mass of the sample. The key contribution in deriving this equation is adding the sensible heat from T_m to T_m^∞ to the enthalpy equation, otherwise eqs 4 and 5 would be the same. The assumption is made that the temperature rise within the melting endotherm does not contribute to the sensible heat. Equation 5 can be rearranged, using eq 3, to yield

$$\begin{aligned} \Delta\hat{H}_m &= \chi_c \left\{ \Delta\hat{H}_m^\infty - \frac{2\sigma}{d\rho_c} \left[1 + \frac{C_{pl}T_m^\infty}{\Delta\hat{H}_m^\infty} \right] \right\} \\ &\equiv \chi_c \left\{ \Delta\hat{H}_m^\infty - \frac{2\sigma}{d\rho_c} [1 + St] \right\} \end{aligned} \quad (6a)$$

where

$$\frac{2\sigma}{d\rho_c} \equiv \frac{2\sigma_e}{L\rho_c} + \frac{2\sigma_s}{h\rho_c} + \frac{2\sigma_f}{w\rho_c} \quad (6b)$$

and Stefan number, St .

$$St = \frac{C_{pl}T_m^\infty}{\Delta\hat{H}_m^\infty} \quad (6c)$$

Mandelkern³⁶ has shown the melting enthalpy of a given sample is affected by the small crystal size even for bulk polyethylene samples. He showed, Figures 9 and 10, that DSC underestimates the degree of crystallinity compared to density and infrared absorption techniques in which the latter two techniques showed remarkable agreement. As shown below, eq 6 can be used to explain that difference with realistic surface energies compared to eq 4.

Equation 6 is a new result not considered before. It will be used to understand the thermal behavior of the mobile-amorphous-free crystals fabricated as part of this study. We first validate its utility by considering the work of Jackson and McKenna³⁹ who studied the effect of pore dimension on the melting behavior of organic solvents. They used a specific form of the GT equation for a material confined in a parallelepiped on four sides and not the other two to arrive at

$$T_m = T_m^\infty \left[1 - \frac{4\sigma_s}{w\rho_c \Delta\hat{H}_m^\infty} \right] \quad (7)$$

where w is the width of the confining sides. Equation 6 will also have a factor of 4 to multiply the surface energy term and is written as

$$\Delta\hat{H}_m^\infty = \chi_c \left\{ \Delta\hat{H}_m^\infty - \frac{4\sigma_s}{w\rho_c} [1 + St] \right\} \quad (8)$$

The data of Jackson and McKenna were analyzed using eqs 7 and 8 assuming $\chi_c = 1$ with results given in Table 1. Error

Table 1. Interpretation of Data from Jackson and McKenna³⁹ Using Eqs 7 and 8^a

	1	2	3 eq 7 (Literature)	4 eq 8 (J-M)	5 eq 7 (J-M)
Compound		St	σ_s (mJ/m ²)	σ_s (mJ/m ²)	σ_s (mJ/m ²)
n-Heptane		3.07	10.0	16.6	13.5
Chlorobenzene		3.30	13.3	17.2	13.3
trans-Decalin		3.89	15.0	15.0	16.2

^aColumns 3 and 5 should yield the same value with the difference being the error in obtaining data from their graphs. Column 4 refers to values computed from the experimental data given by Jackson and McKenna using eq 8.

will result since data were read from graphs given by them, however, the melting enthalpy and temperature agree fairly well with literature values of the bulk. Furthermore, the results presented in columns 3 and 5 should yield the same values and the agreement is adequate given the manner in which the data were obtained here. They did not analyze their melting enthalpy data as done here, and, if they did, the surface energy obtained using eq 4 would be approximately 4–5 times larger since the Stefan number is 3–4 (column 2). We believe the agreement of the surface energy obtained from the melting temperature and enthalpy is good and validates the derivation from the first law of thermodynamics (compare columns 3 and 4) given the *built-in* error associated with data gathering (compare columns 3 and 5).

Further evidence that treating the enthalpy of fusion according to eq 6 is correct comes from the work of Roe and Bair.⁴⁰ In their study, they considered polyethylene and found the surface energy determined via T_m eq 3 to be 4.7 times less than that found from $\Delta\hat{H}_m$ data eq 4. Unfortunately,

the thermodynamic explanation given in their paper was later proven incorrect.⁸ To that end, the Stefan number for polyethylene is approximately 3.5 and would yield a factor of 4.5 difference between the two surface energies according to eq 6. Thus, the difference in the values can be easily explained by the formalism developed here.

Before considering our P3HT crystals, the data for P3HT oligomers are considered first.³² Data for the melting temperature and enthalpy are both given as a function of crystal width allowing comparison between the surface energies obtained from eqs 3 and 6. These are extended chain crystals that are different in form to the chain folded crystals of high molecular weight polymers (although both are Form I crystals³³). Furthermore, the oligomers are slightly polydisperse and have “rough” edges since the longer and shorter molecules cannot directly stack together as, for example, toothpicks would. In our original manuscript³² the amorphous (edge) content was subtracted from the polymer mass to find the enthalpy of melting the crystal with a given crystal length. The correction was done using the peak corresponding to the long period obtained by grazing incidence small angle X-ray scattering.⁴¹

The data are given in Figure 4 and a linear regression is obtained for the melting temperature as a function of inverse

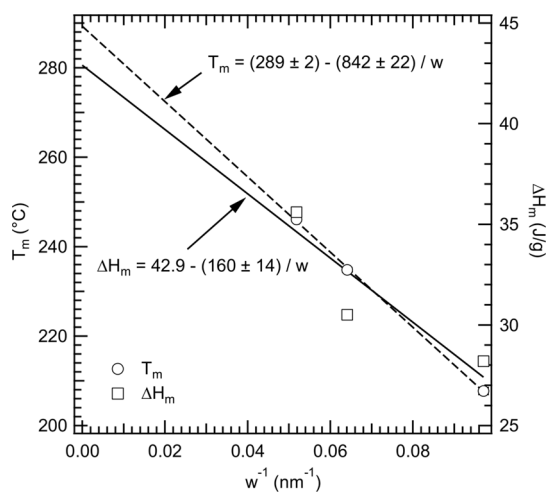


Figure 4. Melting temperature and enthalpy for P3HT oligomers as a function of the inverse crystal width. Data are from Remy et al.³²

crystal width (which is more appropriate than inverse molecular weight in this work). It should be noted, according to Hoffmann and Weeks,⁴² T_m “is determined by warming the specimen at a specified rate by a method which locates the temperature at which the last detectable trace of crystallinity disappears.” Since polymers typically have a distribution of lamellar thicknesses then T_m is the temperature where the thickest crystallite has melted. In the case of the melting enthalpy, the intercept was restrained to give the same value as presented before,³² 42.9 J/g, since more enthalpy data from other literature sources were used to obtain this value. The melting enthalpy of a perfect, infinite P3HT crystal ($\Delta\hat{H}_m^\infty$) has been reported in a wide range from 37 to 99 J/g.^{32,33,43,44} Nevertheless, $\Delta\hat{H}_m^\infty = 42.9$ J/g is employed here for consistency with our previous work. It should also be noted that alternate values of $\Delta\hat{H}_m^\infty$ applied to the mathematical treatment reported in this work produced similar trends. Our reported data, $\Delta\hat{H}_m^\infty = 42.9$ J/g, are close to the data of Snyder

et al.³³ Recently, a value of $\Delta\hat{H}_m^\infty = 75$ J/g⁴⁴ was also reported. Here, we use both data of 42.9 and 75 J/g as reference numbers for our calculation of the surface energy for comparison. Even if the intercept were not constrained very little difference will be seen in the analysis given below.

The surface energy found using eq 3 and the regression shown in the figure is 36 ± 1 mJ/m² with $T_m^\infty = 289 \pm 2$ °C (562 K). Now, using eq 6, one expects to obtain a similar surface energy because of the success of modeling the data of Jackson and McKenna in the previous section. Instead a much lower value is found, 2.9 ± 0.3 mJ/m². The Stefan number is very large for P3HT ($St = 30.1$) since the liquid heat capacity is approximately 2.3 J/g-K and $\Delta\hat{H}_m^\infty$ is 42.9 J/g, respectively. When using a $\Delta\hat{H}_m^\infty$ of 75 J/g, the Stefan number is 17.2. The largeness of the Stefan number could certainly contribute to the small value of surface energy. However, if the Stefan correction is not used then the surface energy becomes 90 mJ/m² with $\Delta\hat{H}_m^\infty = 42.9$ J/g and 249 mJ/m² with $\Delta\hat{H}_m^\infty = 75$ J/g, a very large value. Then, why are these values so different?

One should realize though, the extended chain crystals are essentially infinite in the L direction (see Figure 3) with the exception that there are no chain folds. Like the sheared sample, the h and w are both in nanometer dimensions and this could be the main contributor to this difference in calculated surface energy. In other words, the small dimensions could lead to ill-defined surfaces particularly where the two faces meet at a corner. Furthermore, the crystal faces given by σ_f are ill-defined, because of the inherent polydispersity, and is certainly a poorly defined surface. The fact that the two surface energies do not agree highlights a remaining weakness in our derivation because of limitations in the analysis of such nanoscale surfaces.

Returning to the results for the polymer sample produced after shearing for 24 h, one can also use eq 3 by noting that the melting temperature (as defined by Hoffman and Weeks⁴²) is 233 °C or 506 K and the density of the crystal is 1.13 g/cc (determined by helium pycnometry). The density is in good agreement with the value given by Lee and Dadmun⁴⁵ who determined the crystal density should be between 1.12 and 1.14 g/cc. The result is therefore $\sigma/d = 2.4$ mJ/m²-nm using our values of h and w of 6 and 21 nm, respectively. Taking a simple arithmetic average of these two values results in an average surface energy of 42 mJ/m², similar to the value determined for the oligomers using the same analysis. Here, we utilized the melting enthalpy of an infinitely sized crystal from the literature $\Delta\hat{H}_m^\infty = 42.9$ J/g and $\Delta\hat{H}_m^\infty = 75$ J/g and the melting enthalpy of the mobile-amorphous-free P3HT crystals obtained using shear ($\Delta\hat{H}_m = 25.2$ J/g) to compute their surface energy. Using the melting enthalpy for the mobile-amorphous-free P3HT crystals and eq 6, we found $\sigma/d = 0.32$ mJ/m²-nm and $\sigma/d = 1.55$ mJ/m²-nm and then the average surface energy is 5.7 mJ/m² (much smaller than 90 mJ/m²) and 27.4 mJ/m² (much smaller than 249 mJ/m²), respectively. Again, the two surface energies disagree and follow the same trend as the oligomers. The same argument applies for these crystals formed under shear as was made for the oligomeric P3HT crystals.

While the data of Jackson and McKenna³⁹ could be explained with eqs 3 and 6, these were simple molecules compared to a polymer. Hence the continuum theories may need to be modified as the crystal dimensions shrink and the molecular composition of the crystals under investigation (i.e., small molecules vs. polymers) become more complicated.

CONCLUSIONS

The Gibbs free energy is obtained by a combination of the first and second laws of thermodynamics and is used to determine the relationship of the melting point temperature of finite size crystals to that of an infinite size crystal with the contribution of interfacial energy, eq 3. We derive the new equation here, eq 6, representing the surface energy effect on the enthalpy of fusion that gives, in general, good agreement with the well-known GT equation while still being firmly rooted in thermodynamics. The critical point derived in our equation is a contribution of the *sensible heat* to the melting enthalpy that has not been considered in the past. We proved the effectiveness of our derivation by re-analyzing previously published, highly cited data. In this study, the thermal characteristics of mobile-amorphous-free crystals produced via shear are also analyzed. The average surface energy determined by our melting enthalpy method is smaller than the value obtained by using the traditional melting temperature. It is believed the dimensions of P3HT crystals in multiple directions, in addition to the size of the polymer molecule, contribute to a difference in surface energy values. This difference charts a path forward for further investigation of nanometer scale polymer crystals and the discrepancy in thermodynamic derivations that should largely agree.

AUTHOR INFORMATION

Corresponding Authors

Ngoc A. Nguyen – Department of Materials Science and Engineering, University of Delaware, Newark, Delaware 19716, United States; orcid.org/0000-0002-0278-406X; Email: ngoc.nguyenanh@hust.edu.vn

Michael E. Mackay – Department of Materials Science and Engineering and Department of Chemical and Biomolecular Engineering, University of Delaware, Newark, Delaware 19716, United States; orcid.org/0000-0003-1652-9139; Email: mem@udel.edu

Author

Roddel A. Remy – Department of Materials Science and Engineering, University of Delaware, Newark, Delaware 19716, United States

Complete contact information is available at:
<https://pubs.acs.org/10.1021/acs.macromol.0c02509>

Notes

The authors declare no competing financial interest.

ACKNOWLEDGMENTS

We would like to thank the University of Delaware for the funding through the Department of Materials Science and Engineering, the National Institute of Standards and Technology through the award 70NANB10H256 through the Center for Neutron Science at the University of Delaware, and the W.M. Keck Electron Microscopy Facility at University of Delaware. We thank Prof. Chaoying Ni for assistance with selected area electron diffraction characterization. We also thank Dr. Jeffrey S. Meth at the DuPont Experimental Station for access to the helium pycnometer.

REFERENCES

(1) Pennings, A. J. Polymer crystallization. *J. Phys. Chem. Solids* **1967**, *5*, 389–395.

(2) Pennings, A. J.; Vanderma, J.; Booij, H. C. Hydrodynamically induced crystallization of polymers from solution. 2. Effect of secondary flow. *Kolloid-ZuZPolymere* **1970**, *236*, 99–111.

(3) Pennings, A. J.; Vanderma, J.; Kiel, A. M. Hydrodynamically induced crystallization of polymers from solution. 3. Morphology. *Kolloid-ZuZPolymere* **1970**, *237*, 336–358.

(4) Torfs, J. C. M.; Pennings, A. J. Longitudinal growth of polymer crystals from flowing solutions. VIII. Mechanism of fiber formation on rotor surface. *J. Appl. Polym. Sci.* **1981**, *26*, 303–320.

(5) McHugh, A. Mechanisms of flow induced crystallization. *Polym. Eng. Sci.* **1982**, *22*, 15–26.

(6) McHugh, A. J.; Schultz, J. M. Extensional flow induced crystallization from solution. *Kolloid-Zeitschrift and Zeitschrift Fur Polymere* **1970**, *25*, 193–214.

(7) Pantani, R.; Coccorullo, I.; Speranza, V.; Titomanlio, G. Modeling of morphology evolution in the injection molding process of thermoplastic polymers. *Prog. Polym. Sci.* **2005**, *30*, 1185–1222.

(8) Wunderlich, B., *Macromolecular Physics*. Academic Press: New York, 1980; *3*, 1499.

(9) Sherwood, C.; Price, F.; Stein, R. In Effect of shear on the crystallization kinetics of poly (ethylene oxide) and poly (ε-caprolactone) melts, *Journal of Polymer Science: Polymer Symposia*, **1978**; Wiley Online Library: 1978; 77–94.

(10) Haas, T. W.; Maxwell, B. Effects of shear stress on the crystallization of linear polyethylene and polybutene-1. *Polym. Eng. Sci.* **1969**, *9*, 225–241.

(11) Lagasse, R. R.; Maxwell, B. An experimental study of the kinetics of polymer crystallization during shear flow. *Polym. Eng. Sci.* **1976**, *16*, 189–199.

(12) Kantz, M. R.; Newman, H. D., Jr.; Stigale, F. H. The skin-core morphology and structure–property relationships in injection-molded polypropylene. *J. Appl. Polym. Sci.* **1972**, *16*, 1249–1260.

(13) Karger-Kocsis, J.; Csikai, I. Skin-core morphology and failure of injection-molded specimens of impact-modified polypropylene blends. *Polym. Eng. Sci.* **1987**, *27*, 241–253.

(14) Hobbs, S. Y.; Pratt, C. F. The effect of skin-core morphology on the impact fracture of poly (butylene terephthalate). *J. Appl. Polym. Sci.* **1975**, *19*, 1701–1722.

(15) Kalay, G.; Bevis, M. J. Processing and physical property relationships in injection-molded isotactic polypropylene. 2. Morphology and crystallinity. *J. Polym. Sci. B Polym. Phys.* **1997**, *35*, 265–291.

(16) Kumaraswamy, G.; Verma, R. K.; Issaian, A. M.; Wang, P.; Kornfield, J. A.; Yeh, F.; Hsiao, B. S.; Olley, R. H. Shear-enhanced crystallization in isotactic polypropylene Part 2. Analysis of the formation of the oriented “skin”. *Polymer* **2000**, *41*, 8931–8940.

(17) Wang, Y.; Na, B.; Fu, Q.; Men, Y. Shear induced shish–kebab structure in PP and its blends with LLDPE. *Polymer* **2004**, *45*, 207–215.

(18) Kimata, S.; Sakurai, T.; Nozue, Y.; Kasahara, T.; Yamaguchi, N.; Karino, T.; Shibayama, M.; Kornfield, J. A. Molecular basis of the shish-kebab morphology in polymer crystallization. *Science* **2007**, *316*, 1014–1017.

(19) Keum, J. K.; Zuo, F.; Hsiao, B. S. Formation and stability of shear-induced shish-kebab structure in highly entangled melts of UHMWPE/HDPE blends. *Macromolecules* **2008**, *41*, 4766–4776.

(20) Smith, P.; Lemstra, P. J.; Kalb, B.; Pennings, A. J. Ultrahigh-strength polyethylene filaments by solution spinning and hot drawing. *Polym. Bull.* **1980**, *15*, 505–514.

(21) Smith, P.; Lemstra, P. J. Ultrahigh-strength polyethylene filaments by solution spinning/drawing, 2. Influence of solvent on the drawability. *Macromol. Chem. Phys.* **1979**, *180*, 2983–2986.

(22) Smith, P.; Lemstra, P. J. Ultra-high strength polyethylene filaments by solution spinning/drawing, 3. Influence of drawing temperature. *Polymer* **1980**, *21*, 1341–1343.

(23) Ihn, K. J.; Moulton, J.; Smith, P. Whiskers of poly (3-alkylthiophene) s. *J. Polym. Sci. B Polym. Phys.* **1993**, *31*, 735–742.

(24) Liu, J.; Arif, M.; Zou, J.; Khondaker, S. I.; Zhai, L. Controlling poly (3-hexylthiophene) crystal dimension: nanowhiskers and nanoribbons. *Macromolecules* **2009**, *42*, 9390–9393.

(25) Samitsu, S.; Shimomura, T.; Heike, S.; Hashizume, T.; Ito, K. Effective production of poly (3-alkylthiophene) nanofibers by means of whisker method using anisole solvent: structural, optical, and electrical properties. *Macromolecules* **2008**, *41*, 8000–8010.

(26) Han, Y.; Guo, Y.; Chang, Y.; Geng, Y.; Su, Z. Chain folding in poly (3-hexylthiophene) crystals. *Macromolecules* **2014**, *47*, 3708–3712.

(27) Nguyen, N. A., *Flow induced/refined solution crystallization of a semiconducting polymer*. University of Delaware: 2016.

(28) Wie, J. J.; Nguyen, N. A.; Cwalina, C. D.; Liu, J.; Martin, D. C.; Mackay, M. E. Shear-Induced Solution Crystallization of Poly(3-hexylthiophene) (P3HT). *Macromolecules* **2014**, *47*, 3343–3349.

(29) Koppe, M.; Brabec, C. J.; Heimpl, S.; Schausberger, A.; Duffy, W.; Heeney, M.; McCulloch, I. Influence of Molecular Weight Distribution on the Gelation of P3HT and Its Impact on the Photovoltaic Performance. *Macromolecules* **2009**, *42*, 4661–4666.

(30) Remy, R.; Wei, S.; Campos, L. M.; Mackay, M. E. Three-Phase Morphology of Semicrystalline Polymer Semiconductors: A Quantitative Analysis. *ACS Macro Lett.* **2015**, *4*, 1051–1055.

(31) Noorduyn, W. L.; Vlieg, E.; Kellogg, R. M.; Kaptein, B. From Ostwald ripening to single chirality. *Angew. Chem., Int. Ed.* **2009**, *48*, 9600–9606.

(32) Roddel Remy, E. D. W.; Nguyen, N. A.; Wei, S.; Campos, L. M.; Tomasz Kowalewski, M. E. M. Enthalpy of Fusion of Poly(3-hexylthiophene) by Differential Scanning Calorimetry. *J. Polym. Sci. Part B: Polym. Phys.* **2014**, *52*, 1469–1475.

(33) Snyder, C. R.; Nieuwendaal, R. C.; DeLongchamp, D. M.; Luscombe, C. K.; Sista, P.; Boyd, S. D. Quantifying crystallinity in high molar mass poly (3-hexylthiophene). *Macromolecules* **2014**, *47*, 3942–3950.

(34) Kaptay, G. The Gibbs equation versus the Kelvin and the Gibbs-Thomson equations to describe nucleation and equilibrium of nano-particles. *J. Nanosci. Nanotechnol.* **2011**, *12*, 1–12.

(35) Gibbs, J. W., *The collected works of J. Willard Gibbs (Gibbs never derived the Gibbs-Thomson equation, it can be derived from eqn (659) on page 315 of this book)*. Yale University Press: New Haven: 1948.

(36) Mandelkern, L. Thermodynamic and morphological properties of bulk crystallized polymers. *Polym. Eng. Sci.* **1967**, *7*, 232–252.

(37) Zhou, H.; Wilkes, G. L. Comparison of lamellar thickness and its distribution determined from dsc, SAXS, TEM and AFM for high-density polyethylene films having a stacked lamellar morphology. *Polymer* **1997**, *38*, 5735–5747.

(38) Alberola, N.; Cavaille, J. Y.; Perez, J. Mechanical spectrometry of alpha relaxations of high-density polyethylene. *J. Polym. Sci. B Polym. Phys.* **1990**, *28*, 569–586.

(39) Jackson, C. L.; McKenna, G. B. The melting behavior of organic materials confined in porous solids. *J. Chem. Phys.* **1990**, *93*, 9002–9011.

(40) Roe, R.-J.; Bair, H. E. Thermodynamic Study of Fold surfaces of Polyethylene Single Crystals. *Macromolecules* **1970**, *3*, 454–458.

(41) Zhang, R.; Li, B.; Iovu, M. C.; Jeffries-el, M.; Sauv e, G.; Cooper, J.; Jia, S.; Tristram-Nagle, S.; Smilgies, D. M.; Lambeth, D. N. Nanostructure dependence of field-effect mobility in regioregular poly (3-hexylthiophene) thin film field effect transistors. *J. Am. Chem. Soc.* **2006**, *128*, 3480–3481.

(42) Hoffman, J. D.; Weeks, J. J. Melting process and the equilibrium melting temperature of polychlorotrifluoroethylene. *J. Res. Natl. Bur. Stand A* **1962**, *66*, 13–28.

(43) Malik, S.; Nandi, A. K. Crystallization mechanism of regioregular poly (3-alkyl thiophene) s. *J. Polym. Sci. B Polym. Phys.* **2002**, *40*, 2073–2085.

(44) Alizadehghadam, M.; Heck, B.; Siegenf uhr, S.; Abbasi, F.; Reiter, G. Thermodynamic Features of Perfectly Crystalline Poly (3-hexylthiophene) Revealed through Studies of Imperfect Crystals. *Macromolecules* **2019**, *52*, 2487–2494.

(45) Lee, C. S.; Dadmun, M. D. Important thermodynamic characteristics of poly (3-hexyl thiophene). *Polymer* **2014**, *55*, 4–7.